Published in final edited form as:

Langmuir. 2019 February 05; 35(5): 1440–1449. doi:10.1021/acs.langmuir.8b01633.

Zwitterionic Cross-Linked Biodegradable Nanocapsules for Cancer Imaging

Haotian Sun[†], **Lingyue Yan**[‡], **Kevin A. Carter**[‡], **Jiaqi Zhang**[†], **Julia Caserto**[†], **Jonathan F. Lovell**[‡], **Yun Wu**[*,‡], **Chong Cheng**[*,†]

[†]Department of Chemical and Biological Engineering, University at Buffalo, The State University of New York, Buffalo, New York, 14260, USA.

[‡]Department of Biomedical Engineering, University at Buffalo, The State University of New York, Buffalo, New York, 14260, USA.

Abstract

Biodegradable crosslinked zwitterionic nanocapsules were synthesized for cancer imaging. A polylactide (PLA)-based diblock copolymer with two blocks carrying acetylenyl and allyl groups respectively was synthesized by ring-opening polymerization (ROP). Azide-alkyne “click” reaction was conducted to conjugate sulfobetaine (SB) zwitterions and fluorescent dye Cy5.5 onto the acetylenyl-functionalized first block of the diblock copolymer. The resulting copolymer with a hydrophilic SB/Cy5.5-functionalized PLA block and a hydrophobic allyl-functionalized PLA block could stabilize miniemulsions because of its amphiphilic diblock structure. UV-induced thiol-ene “click” reaction between a dithiol crosslinker and the hydrophobic allyl-functionalized block of the copolymer at the peripheral region of nanoscopic oil droplets in miniemulsion generated crosslinked polymer nanocapsules (NCs) with zwitterionic outer shells. These NCs showed an average hydrodynamic diameter (D_h) of 136 nm. They exhibited biodegradability, biocompatibility and high colloidal stability. *In vitro* study indicated that these NCs could be taken up by MIA PaCa-2 cancer cells. *In vivo* imaging study showed that, comparing to a small molecule dye, NCs had a longer circulation time, facilitating their accumulation at tumors for cancer imaging. Overall, this work demonstrates the applicability of biodegradable zwitterionic polymer-based materials in cancer diagnosis.

Graphical Abstract

[*]**Corresponding Author** Authors to whom correspondence should be addressed: ccheng8@buffalo.edu (C. Cheng); ywu32@buffalo.edu (Y. Wu).

Supporting Information.

The Supporting Information is available free of charge on the ACS Publications website at DOI:. Figure S1-S6 (PDF)

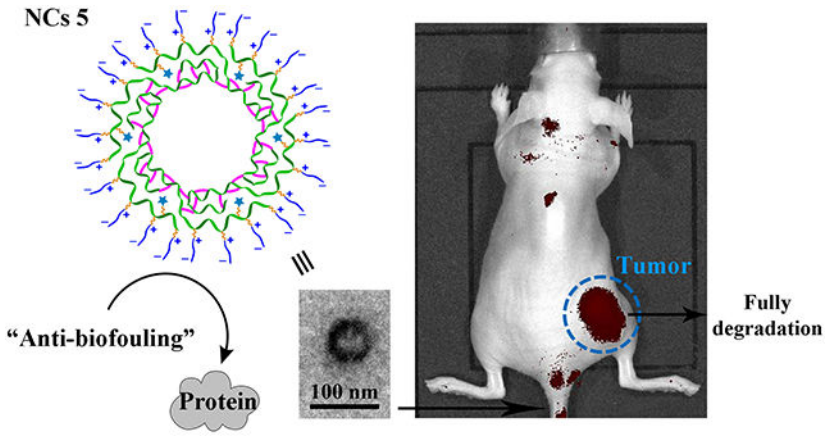

Keywords

zwitterionic polymer; biodegradable polymer; miniemulsion crosslinking; nanocapsules; cancer imaging

INTRODUCTION

Polymer nanocapsules (NCs) are polymer nanoparticles (NPs) with inner cavities.[1] Their special hollow core structure makes them promising for various applications such as drug delivery and controlled release of various cargoes.[2, 3] Crosslinked NCs have drawn significant attention because their covalently crosslinked shell architectures effectively enhance their structural stability.[4] Robust crosslinked NCs have been employed as containers with persistent structures for therapeutic delivery (including drug,[5, 6] gene,[7] and protein[8]), medical imaging,[9, 10] and "nanoreactors"[11].

Crosslinked NCs can be prepared by the cavitation of pre-prepared shell-crosslinked nanostructures, vesicular crosslinking, and emulsion-based interfacial crosslinking.[4] The emulsion-based approaches often just require relatively simple components, and allow directly *in situ* encapsulation of cargoes. More specifically, miniemulsions can be employed as templates to prepare crosslinked NCs.[12] For instance, we demonstrated the preparation of crosslinked NCs by highly efficient UV-induced thiol-ene "click" crosslinking of precursor polymers with surfactant properties in transparent miniemulsions in our previous studies.[5, 13, 14] By using amine-functionalized cationic polylactide (PLA) as the precursor polymer, cationic NCs with well-defined covalently stabilized biodegradable structures were obtained, and *in vitro* studies showed that they can overcome multidrug resistance and enable individual and co-delivery of drug and gene to cancer cells.[13, 15] Moreover, other features of these cationic NCs, such as biodegradability and biocompatibility, also enhance their promising applicability for therapeutic delivery.[16]

Recently, zwitterionic materials have been widely studied for biological applications mainly because of their biocompatibility and anti-biofouling properties, which can enable long blood circulation time.[17, 18] The incorporation of biodegradability with zwitterionic materials can minimize their long-term side effects in biological environments, and

therefore, is important for enhancing their biomedical applicability.[19] However, most of the reported zwitterionic materials were derived from zwitterionic (meth)acrylic esters or amides, and therefore, do not possess biodegradability. Taking advantage of the thiol-ene "click" chemistry using a biodegradable PLA-based precursor polymer, recently we reported a fully degradable zwitterionic polymer by thiol-ene reaction of thiol-functionalized sulfobetaine (SB) zwitterion with allyl-functionalized PLA.[20] The conjugate of the SB-functionalized zwitterionic PLA with paclitaxel, a potent anticancer drug, was also studied for sustained drug delivery.

Fluorescent dye-doped NPs have attracted significant attention for biomedical imaging applications, because they are brighter and more photostable than conventional organic fluorescence probes.[21] Similar to drug delivery systems, NPs for biomedical imaging also require thoughtful design considerations on structure and properties of the scaffolds, according to the required biological environments.[22] In principle, the unique combination of biomedical relevant properties of biodegradable zwitterionic polymers makes them to be promising scaffold materials for biomedical imaging. Herein, we report novel fluorescent dye-doped crosslinked NCs derived from zwitterionic SB-functionalized PLA for cancer imaging (Scheme 1). Besides the favorable properties from the biodegradable zwitterionic precursor polymer, such NCs were designed to have not only nanoscopic dimensions to capitalize enhanced permeability and retention (EPR) effect which leads to accumulation of NCs at tumor site, but also inner cavities which potentially can be utilized for the delivery of therapeutic cargoes. A special SB zwitterion modified with an azide group (SB-N_3, **1**) was designed and synthesized. Functional PLAs, including acetylenyl-functionalized PLA **2** and diblock PLA **3** with both acetylenyl- and allyl-functionalized blocks, were prepared successively by ring-opening polymerization (ROP). Azide-alkyne "click" reaction of **1** and cyanine5.5 azide (Cy5.5-N_3), an azide-modified fluorescent dye, with the acetylenyl-functionalized first block of **3** was performed to yield **4** with both SB and Cy5.5 conjugated to its first block.[23] Then **4** was used to prepare NCs by miniemulsion cross-linking *via* UV-induced thiol-ene "click reaction". The resulting NCs **5** were demonstrated to be promising cancer imaging agents with high colloidal stability, biodegradability, and biocompatibility. *In vivo* imaging and biodistribution study also demonstrated that **5** could be used for cancer imaging.

EXPERIMENTAL SECTION

Materials.

3-Dimethylamino-1-propyl chloride hydrochloride (98%) and 1,3-propanesultone (99%) were purchased from Alfa Aesar. Sodium azide (99%), 2,2-dimethoxy-2-phenylacetophenone (DMPA, 99%), and sodium periodate (99%) were purchased from Acros Organics. Magnesium sulfate anhydrous ($MgSO_4$), sodium hydroxide (NaOH, pellets), L-ascorbic acid sodium salt (NaAsc), and copper sulfate pentahydrate ($CuSO_4$•$5H_2O$) were purchased from Fisher Scientific. (3*S*)-*cis*-3,6-Dimethyl-1,4-dioxane-2,5-dione (L-LA, 98%), 4-(dimethylamino)pyridine (DMAP, 99%, prilled), and fibrinogen from human plasma were purchased from Sigma-Aldrich. Benzyl alcohol (BnOH) was purchased from J. T. Baker. Cyanine5.5 azide (Cy5.5-N_3) was purchased

from Lumiprobe Corporation. 1,4-Butanediol bis(3-mercaptopropionate) was purchased from Fujifilm Wako Chemical Corporation. Ruthenium dioxide (99.9%) was purchased from Pfaltz & Bauer. Fetal bovine serum (FBS, qualified, USDA-approved regions) was purchased from Life Technologies. Hexanes (HPLC grade), ethyl acetate (HPLC grade), dichloromethane (DCM, HPLC grade), chloroform (HPLC grade), methanol (HPLC grade), diethyl ether (HPLC grade), acetone (Certified ACS grade), and *N,N*'-dimethylformamide (DMF; HPLC grade) were purchased from Fisher Scientific. DCM and DMF were dried by distillation over CaH_2 before use. Acetylenyl-functionalized lactide (ACLA) and allyl-functionalized lactide (ALLA) were freshly synthesized following our previous publications.[14, 24]

Synthesis of 3-azido-*N,N*-dimethylpropan-1-amine.

The reaction was conducted according to the literature with some changes.[25, 26] To a round-bottom flask equipped with a reflux condenser was added 3-dimethylamino-1-propyl chloride hydrochloride (1.58 g, 10.0 mmol, 1.00 eq), sodium azide (1.30 g, 20.0 mmol, 2.00 eq) and 20 mL H_2O. The solution was heated to 80 °C for 23 h. After cooling to room temperature, 1 M NaOH was added slowly until the solution reached pH of ~10. Then the solution was extracted by diethyl ether for three times. The organic layers were collected, combined, and dried with $MgSO_4$. After evaporation, the pure product was obtained as a colorless oil (0.84 g, 65% yield). Noteworthily, because organic azides can be explosive, the reaction must be conducted very carefully. ^{1}H NMR (500 MHz, $CDCl_3$, δ): 3.34 (t, 2H, $CH_2CH_2CH_2N_3$), 2.34 (t, 2H, $CH_2CH_2CH_2N_3$), 2.22 (s, 6H, $N(CH_3)_2$), 1.75 (m, 2H, $CH_2CH_2CH_2N_3$).

Synthesis of SB-N_3 (1).

The reaction was conducted according to the literature with some changes.[20] In a 10 mL glass vial, 1,3-propanesultone (362 mg, 2.97 mmol, 0.95 eq) was dissolved in 3 mL dry acetone under nitrogen atmosphere. Then 3-azido-*N,N*-dimethylpropan-1-amine (400 mg, 3.12 mmol, 1.00 eq) was slowly added to the solution. After a few minutes, white solid powders started to appear in the solution. The mixture was stirred at room temperature for 46 h in total. After filtration, the solid was washed with a large amount of acetone. After drying under vacuum, finally the pure product was obtained as a white solid (0.60 g, 80%). ^{1}H NMR (500 MHz, D_2O, δ): 3.43-3.28 (m, 6H, $SO_3CH_2CH_2CH_2$ and $CH_2CH_2CH_2N_3$), 3.01 (s, 6H, $N(CH_3)_2$), 2.87 (t, 2H, $SO_3CH_2CH_2CH_2$), 2.17-2.07 and 2.01-1.91 (m, 4H, $SO_3CH_2CH_2CH_2$ and $CH_2CH_2CH_2N_3$).

Synthesis of Acetylenyl-Functionalized PLA (2).

ROP of LA (348 mg, 2.42 mmol) with ACLA (610 mg, 3.63 mmol) was conducted by using BnOH (13.1 mg, 0.12 mmol) as the initiator and DMAP (59.1 mg, 0.48 mmol) as the organocatalyst in dry DCM ($[LA]_0$:$[ACLA]_0$:$[BnOH]_0$:$[DMAP]_0$ = 20:30:1:4). The reaction mixture was stirred for 5 days under N_2 atmosphere at 35 °C. The product was precipitated twice in large amounts of cold methanol to remove the unreacted monomer and the organocatalyst DMAP. Finally, polymer **2** was obtained as a white solid (0.60 g, 63%). ^{1}H NMR analysis indicated the formula of **2** as poly($LA_{0.46}$-*co*-$ACLA_{0.54}$)$_{75}$. ^{1}H NMR (500

MHz, $CDCl_3$, δ): 7.41-7.31 (m, Ar-*H* from BnOH), 5.45-5.06 (br m, C*H*CH_3 of LA units; C*H*CH_3, C*H*CH_2C≡CH of ACLA units), 3.02-2.66 (br m, CHC*H*$_2$C≡CH of ACLA units), 2.15-1.99 (br s, $CHCH_2$C≡C*H* of ACLA units), 1.67-1.40 (br m, CHC*H*$_3$ of LA and ACLA units). M_n^{NMR} = 11.9 kDa, M_n^{GPC} = 24.9 kDa, $Đ^{GPC}$ = 1.10.

Synthesis of Acetylenyl/Allyl-Functionalized Diblock PLA (3).

ROP of LA (66 mg, 0.46 mmol) with ALLA (92 mg, 0.54 mmol) was conducted with copolymer **2** (158 mg, 0.0133 mmol) as the polymeric initiator, DMAP (6.5 mg, 0.053 mmol) as the organocatalyst, and followed this condition: $[LA]_0$:$[ALLA]_0$:$[\mathbf{2}]_0$:$[DMAP]_0$ = 34.5:40.5:1:4 in dry DCM. The reaction mixture was stirred for 8 days under N_2 atmosphere at 35 °C. The product was precipitated twice in large amounts of cold methanol to remove the unreacted monomers and the organocatalyst DMAP. Finally, diblock polymer **3** was obtained as a white solid (114 mg, 36% yield). ^{1}H NMR analysis indicated the formula of **3** as poly($LA_{0.46}$-*co*-$ACLA_{0.54}$)$_{75}$-*b*-poly($LA_{0.74}$-*co*-$ALLA_{0.26}$)$_{18}$. ^{1}H NMR (500 MHz, $CDCl_3$, δ): 7.41-7.31 (m, Ar-*H* from BnOH), 5.91-5.69 (m, CH_2C*H*=CH_2 of ALLA units), 5.45-5.05 (br m, C*H*CH_3 of LA units; C*H*CH_3, C*H*CH_2C≡CH of ACLA units; C*H*CH_3, C*H*CH_2CH=C*H*$_2$ of ALLA units), 3.05-2.75 (br m, CHC*H*$_2$C≡CH of ACLA units), 2.75-2.47 (br m, CHC*H*$_2$CH=CH_2 of ALLA units), 2.14-1.99 (br s, $CHCH_2$C≡C*H* of ACLA units), 1.78-1.39 (br m, CHC*H*$_3$ of LA, ACLA and ALLA units). M_n^{NMR} = 14.6 kDa, M_n^{GPC} = 28.3 kDa, $Đ^{GPC}$ = 1.09.

Synthesis of SB/Cy5.5/Allyl-Functionalized Diblock PLA (4).

Azide-alkyne click reaction was conducted to conjugate both SB-N_3 and Cy5.5-N_3 onto the PLA backbone of **3**. The feed ratio was [acetylenyl group of **3**]$_0$:[SB-N_3]$_0$:[Cy5.5-N_3]$_0$:[$CuSO_4$•$5H_2O$]$_0$:[NaAsc]$_0$ = 40.5:38.3:1.0:1.8:3.6. A mixture of DMF and H_2O (v/v = 8:1) was used as the reaction solvent. In a 10 mL flask, **3** (72.3 mg) and Cy5.5-N_3 (3.4 mg) were added with 4.0 mL of DMF; SB-N_3 (47.4 mg) and NaAsc (3.5 mg) were added with 0.4 mL of water. Then the flask was filled with N_2, followed by the addition of $CuSO_4$•$5H_2O$ (2.2 mg) with 0.1 mL H_2O using syringe. Three freeze-pump-thaw cycles were performed to further remove oxygen in the reaction system. The reaction mixture was stirred for 21 h at room temperature. The crude product was dialyzed against acetone and DCM:MeOH (v/v = 5:1), respectively, to remove the unreacted SB-N_3 and Cy5.5-N_3. The product was obtained as a blue solid after filtration, followed by drying under vacuum. finally filtrated to remove the salts, yielding 112 mg of **4** with 94.4% yield. ^{1}H NMR (500 MHz, $CDCl_3$/CD_3OD (v/v, 1:1), δ): 8.08-7.72 (br m, $CHCH_2$C=C*H*N), 7.38-7.27 (m, Ar-*H* from BnOH), 5.88-5.69 (br m, $CHCH_2$C*H*=CH_2 of ALLA units), 5.57-5.35 (br m, C*H*CH_2C=CHN), 5.34-4.92 (br m, C*H*CH_3, and C*H*CH_2CH=C*H*$_2$ of ALLA units; C*H*CH_3 of LA and ACLA units), 4.58-4.42 (br m, NC*H*$_2$$CH_2$$CH_2N(CH_3)_2$), 3.66-3.20 (br m, NCH_2CH_2C*H*$_2$N$(CH_3)_2$, NC*H*$_2$$CH_2$$CH_2$$SO_3$, and CHC*H*$_2$C=CHN), 3.18-3.01 (br m, $NCH_2CH_2CH_2$N(C*H*$_3$)$_2$), 2.93-2.76 (br m, NCH_2CH_2C*H*$_2$$SO_3$, and CHC*H*$_2$C≡CH of ACLA units), 2.76-2.55 (br m, CHC*H*$_2$CH=CH_2 of ALLA units), 2.53-2.35 (br m, NCH_2C*H*$_2$$CH_2N(CH_3)_2$), 2.20-2.04 (br m, NCH_2C*H*$_2$$CH_2$$SO_3$), 2.04-1.96 (br s, $CHCH_2$C≡C*H* of ACLA units), 1.65-1.35 (br m, C*H*$_3$ of units on PLA backbone). M_n^{NMR} = 24.7 kDa.

Synthesis of Crosslinked SB/Cy5.5-Functionalized PLA-based NCs (5).

In a 8 mL vial, a chloroform solution (0.057 mL) containing 1,4-butanediol bis(3-mercaptopropionate) (0.70 mg, with 1.3 eq of thiol groups) and DMPA (0.12 mg, 0.1 eq) was added to 2.83 mL of water solution of **4** (21.9 mg, with 1.0 eq of allyl groups). Ultrasonication (Branson Sonifier 250, output: 1, duty cycle: 50%) was performed for 20 min to generate a transparent oil-in-water (O/W) miniemulsion. Then UV irradiation (λ_{max} = 365 nm) was conducted for 30 min at room temperature to induce thiol-ene cross-linking reaction. Finally, the aqueous solution of crosslinked SB/Cy5.5-functionalized NCs ([Cy5.5] = 0.2 mg/mL) was obtained after removal of chloroform using rotavapor. During the synthetic process, samples were taken after each step for nanoparticle tracking analysis (NTA) to monitor the size change.

Characterization Methods.

^{1}H NMR spectra were recorded using a 500 MHz Varian INOVA-500 spectrometer at 25 °C, using $CDCl_3$ (with tetramethylsilane as an internal standard), D_2O, or CD_3OD as the solvent. Gel permeation chromatography (GPC) was used to determine the number-average molecular weight (M_n) and molecular weight dispersity ($Đ$) of functionalized PLAs **2** and **3**. A Viscotek GPC system equipped with a VE-1122 pump, a VE-3580 refractive index (RI) detector, and a VE-3210 UV/Vis detector was employed. Two mixed-bed organic columns (PAS-103M-UL and PAS-105M-M) were used in the GPC system, with DMF containing 0.01 M LiBr as the eluent (flow rate: 0.5 mL/min, at 55 °C). Both **2** and **3** were dissolved in DMF at a concentration of ~3 mg/mL, and the injection volume was 0.1 mL for each measurement. Linear polystyrene standards ($Đ$ < 1.1) purchased from Varian were used for calibration. NTA was used to determine hydrodynamic diameters (D_h) of assembled NPs of **4** and crosslinked NCs **5**.[27] The measurements were performed on NanoSight LM10 (Malvern Instruments, laser wavelength: 405 nm). Brownian motions of the NPs and the NCs (1 mg/mL) in different aqueous environment were recorded and tracked, from which the size data of each sample were generated. Transmission electron microscopy (TEM) images of assembled NPs of **4** and crosslinked NCs **5** were obtained with a JEOL 2010 microscope. Their dilute solutions in water (0.1 mg/mL) were dip coated onto the 400 mesh carbon-coated copper TEM grids. After complete drying under vacuum, the samples were stained by freshly prepared 0.5% solution of ruthenium tetroxide (RuO_4). The staining agent was prepared by the reaction between ruthenium dioxide and sodium periodate in water for 1 h. The staining process lasted for 3 h before measurements.

Cell Culture.

MIA PaCa-2 ATCC® CRL-1420™ (PaCa-2 for short) cells were purchased from the American Type Culture Collection (Manassas, VA). PaCa-2 cells were cultured in DMEM supplemented with 10% fetal bovine serum (FBS, Life Technologies), 1% penicillin-streptomycin and 1% sodium pyruvate (Invitrogen, 11360070) at 37 °C with 5% CO_2.

In Vitro Cell Viability.

The cytotoxicity of NCs **5** was evaluated based on the viability of PaCa-2 cells. The cells were seeded in 96 wells plates (Greiner Bio-one, 655180) at the seeding density of 1×10^4

cells per well in 100 μl cell culture medium. The cells were allowed to grow overnight at 37 °C with 5% CO_2. The solutions of NCs **5** at different concentrations were prepared in cell culture medium to treat cells at final concentrations of 50, 75, 100, 200, 300 and 500 μg/mL. AlamarBlue (Invitrogen, DAL1025) was used to measure the viability of PaCa-2 cells at 72 h after treatment following the manufacturer's protocol. Briefly, one part of AlamarBlue reagent was added to 10 parts of cell culture medium. The mixture was then added to cells and incubated at 37 °C for 3 h, protected from light. Fluorescence intensity was measured using TECAN microplate reader (San Jose, CA). The excitation and emission wavelengths were set at 560 nm and 590 nm, respectively. The cell viability was normalized to PBS treated groups.

In Vitro Cellular Uptake Analysis.

PaCa-2 cells were seeded in 6-well plates (Greiner Bio-one, 655180) at 2×10^5 cells per well and allowed to grow overnight. The cells were then treated with Cy5.5-N_3 and NCs **5** at Cy5.5 concentration of 0.2 μg/mL. Untreated cells were the controls. At 24 h of post treatment, the cells were harvested and fixed in 4% paraformaldehyde (Acros, 41678-5000) for analysis by flow cytometry and confocal microscopy. The flow cytometry analysis was conducted by a BD Fortessa flow cytometer (BD bioscience, San Jose, CA) in the APC channel (λ_{ex} = 640 nm and λ_{em} = 660 nm). For each sample, 10,000 events were collected. The mean fluorescence intensity ± standard deviation of Cy5.5 were reported to illustrate cellular uptake. For confocal microscopy imaging, the cell nuclei were counter stained with DAPI (Sigma Aldrich, D8417). Then the cells were mounted on glass slides and imaged using LSM 710 confocal microscope (ZEISS, Dublin, CA) through the DAPI channel (λ_{ex} = 405 nm and λ_{em} = 497.5 nm) and Cy5 channel (λ_{ex} = 640 nm and λ_{em} = 701.5 nm), respectively.

In Vivo Imaging and Biodistribution.

5×10^6 PaCa-2 cells were injected subcutaneously at the flanks of female athymic nude mice (6-week old, Charles River Laboratories). When tumor volume reached ~300 mm^3, the mice were divided into three groups and treated with 0.9% saline (control), Cy5.5-N_3 in 0.9% saline and NCs **5** in 0.9% saline, respectively, through intravenous injection at Cy5.5 dose of 1.5 mg/kg of body weight. Whole body Cy5.5 fluorescence images (λ_{ex} = 675 nm and λ_{em} = 720 nm) were taken by IVIS Lumina II *in vivo* imaging system (PerkinElmer, Waltham, MA) before and 5 min, 1 h, 4 h, 24 h after injection.[28] Then the mice were euthanized. Tumor and major organs (including brain, heart, liver, spleen, lung and kidney) were harvested. The fluorescence images of organs was recorded and quantified by using the IVIS *in vivo* imaging system. The animal protocol was approved by the University at Buffalo Institutional Animal Care and Use Committee (IACUC).

RESULTS AND DISCUSSION

Synthesis and Chemical Characterization.

The synthesis of crosslinked SB/Cy5.5-functionalized PLA-based NCs is illustrated in Scheme 1. An azide-functionalized small-molecule zwitterion, SB-N_3 (**1**), was prepared *via* a two-step organic synthesis in which the nucleophilic substitution reaction of 3-

dimethylamino-1-propyl chloride with sodium azide was performed at first, followed by the reaction of the resulting 3-azido-*N,N*-dimethylpropan-1-amine with 1,3-propanesultone. Compound **1** was obtained with an overall yield of 52%, and its high purity was illustrated by ^{1}H NMR analysis (Figure S1).

The diblock PLA backbone (**3**) was synthesized by a two-step ROP process. The first step was ROP of LA and ACLA initiated by BnOH and organocatalyzed by DMAP at 35 °C for 5 days ($[LA]_0$:$[ACLA]_0$:$[BnOH]_0$:$[DMAP]_0$ = 20:30:1:4), to give acetylenyl-functionalized PLA **2** in 63% yield after purification. ^{1}H NMR analysis revealed that **2** was composed of 46 mol% of LA and 54 mol% of ACLA (Figure S2a), according to the areas of peak b (COOCH of LA and ACLA units) at 5.06-5.45 ppm, peak *f* ($CHCH_2C{\equiv}CH$ of ACLA units) at 2.66-3.02 ppm and peak *g* ($CHCH_2C{\equiv}CH$ of ACLA units) at 1.99-2.15 ppm. The total degree of polymerization (DP) of 75 was determined for **2** (40.5 for ACLA units, 34.5 for LA unit), based upon the comparison of the area of peak b with the area of peak for *Ar-H* (from terminal Bn group) at 7.31-7.41 ppm. The second step was ROP of LA with ALLA using **2** as the initiator and DMAP as the organocatalyst at 35 °C for 8 days ($[LA]_0$:$[ALLA]_0$:$[\mathbf{2}]_0$:$[DMAP]_0$ = 34.5:40.5:1:4). The diblock functional PLA **3** was obtained in 36 % yield after purification, and the relatively low yield was ascribed to the decreased reactivity of active polymer terminals with the increase of polymer chain length. According to ^{1}H NMR analysis, the allyl-functionalized second PLA-based block of **3** was composed of 74 mol% of LA and 26 mol% of ACLA (Figure S2b). The number of ALLA units was determined as 4.6 by comparing the areas of peak *d* ($CH_2CH{=}CH_2$ of ALLA units) and peak *g* ($CHCH_2C{\equiv}CH$ of ACLA units), based on the assumption that the first acetylenyl-functionalized block of **3** was identical with precursor **2** regarding chain length and composition. Then the number of LA units in the second block was determined as 13.5 by comparing the areas of peak *d* ($CH_2CH{=}CH_2$ of units from ALLA) with peak *a* ($CHCH_3$ of LA units from both blocks; $CHCH_3$ of 4.6 ALLA units and 40.5 ACLA units), respectively. Thus, with a DP of 18 for its second block, diblock copolymer **3** had an overall DP of 93. GPC analysis revealed well-controlled chain growth and extension in the ROP process, and polymers **2** and **3** had narrow molecular weight dispersity (Đ) of 1.10 and 1.09, respectively, relative to linear polystyrenes (Figure S3).

The highly efficient azide-alkyne click chemistry was employed to react both SB-N_3 (**1**) and Cy5.5-N_3 with acetylenyl groups of **3** using $CuSO_4{\bullet}5H_2O$/NaAsc as the catalytic system in DMF/H_2O (v/v = 8:1) mixed solvent at room temperature for 21 h ([acetylenyl group of **3**]$_0$: [SB-N_3]$_0$:[Cy5.5-N_3]$_0$:[$CuSO_4{\bullet}5H_2O$]$_0$:[NaAsc]$_0$ = 40.5:38.3:1.0:1.8:3.6). After the azide-alkyne reaction, the reaction solution was analyzed by DMF GPC. The resulting diblock copolymer **4** with a hydrophilic SB/Cy5.5-functionalized PLA block and a hydrophobic allyl-functionalized PLA block showed very low solubility in DMF due to its amphiphilic property,[20, 29] and only a very weak GPC curve of the crude product of **4** was observed by using RI detector (Figure S3b). On the other hand, the more visible GPC peak of **4** obtained by using UV/Vis detector (wavelength 684 nm) indicated the presence of conjugated Cy5.5 moiety in **4** as a result of successful azide-alkyne conjugation reaction (Figure S3b). Comparison of UV/Vis signal intensity of **4** with that of the unreacted Cy5.5-N_3 indicated ~67% conversion of Cy5.5-N_3 in the reaction, which should be a lower limit of conversion

because Cy5.5-N_3 is more soluble than **4** in DMF. After separation by dialysis, **4** was obtained in 94.4% yield, based on the mass of the recovered polymer. ^{1}H NMR analysis revealed 31.3 wt% of SB moieties in **4** (Figure 1), corresponding to 74% conversion of SB-N_3 in the azide-alkyne reaction. The number of SB conjugated ACLA units was determined as 31.1 by comparing the areas of peak *Ar-H* (from Bn) with peak *i* ($NCH_2CH_2CH_2N(CH_3)_2$ of units from SB). The number was also confirmed by comparing the areas of peak *Ar-H* with peak *g* ($CHCH_2C{\equiv}CH$ of units from ACLA). Meanwhile, according to the intensities of the ^{1}H NMR resonances from allyl protons, ^{1}H NMR analysis indicated that allyl groups from **3** were completely intact during the azide-alkyne reaction, and therefore, they were available for the synthesis of CPNCs via thiol-ene crosslinking.

Amphiphilic diblock PLA **4** can effectively stabilize water-oil interface because its hydrophilic SB/Cy5.5-functionalized block and hydrophobic allyl-functionalized block can effectively affiliate with water and oil phase, respectively. Transparent miniemulsion was readily obtained by ultrasonication of a mixture consisting of water (~98 vol%), chloroform (as oil; ~2 vol%), **4**, 1,4-butanediol bis(3-mercaptopropionate) (as dithiol crosslinker), and DMPA (as photoinitiator) for 20 min ($[thiol]_0$:[allyl of **4**]$_0$:$[DMPA]_0$ = 1.3:1.0:0.1). Subsequently, thiol-ene crosslinking reaction was performed by UV-irradiation (λ_{max} = 365 nm) of the transparent miniemulsion for 30 min, converting **4** to crosslinked SB/Cy5.5-functionalized PLA-based NCs **5**. A sample of the final NCs solution was freeze-dried and analyzed by ^{1}H NMR. The absence of the resonance of the C*H* proton from allyl groups at 5.88-5.69 ppm confirmed that all the allyl groups were consumed during the thiol-ene reaction process, forming crosslinked structures (Figure 2a).

Nanostructure Characterization.

Nanostructures were involved for both SB/Cy5.5/allyl-functionalized diblock PLA **4** and the derived crosslinked NCs **5**. While NCs **5** possess covalently stabilized unimolecular nanostructure, the amphiphilic diblock PLA **4** forms nanoparticles (NPs) through self-assembly in selective solvents. The assembled NPs of **4** and the crosslinked NCs **5** were characterized by both NTA and TEM, respectively, to reveal their structural features. Dynamic light scattering (DLS) was not employed in this study because the excitation and emission spectra of Cy5.5 can interfere with the 4 mM 633 nm laser of the Zetasizer Nano ZS90 (Malvern Instruments Ltd.).[30] NTA showed that NPs of **4** had an average hydrodynamic diameter (D_h) of 84 nm (with the peak of the profile at 72 nm) (Figure 3a). The size of NPs of **4** was larger than a previously reported zwitterionic sulfobetaine polymer (hydrodynamic diameter: 14.4 ± 0.1 nm) without amphiphilic diblock structure.[20] TEM image of NPs of **4** showed spherical NPs with number-average diameter of 38.2 ± 2.3 nm (Figure 2b). For NCs **5**, NTA showed an average hydrodynamic diameter (D_h) of 136 nm (with the peak of the profile at 124 nm) (Figure 3b), which was larger than that of NPs of **4** (Figure 3c). TEM images of NCs **5** confirmed that the morphology of these NCs as spherical NPs with inner cavities (Figure 2c, Figure S4). The number-average diameter of NCs **5** was determined to be 92.1 ± 18.4 nm.

Noteworthily, NTA was also used to monitor the miniemulsion crosslinking synthesis of NCs **5** (Figure 3c). Before cross-linking, the average D_h of oil nanodroplets stabilized by **4**

was 135 nm. After cross-linking, the average D_h of oil nanodroplets encapsulated by NCs **5** was 157 nm. After the removal of chloroform, the final NCs **5** dispersed in water showed an average D_h of 136 nm. The fact that the nanodroplets and the resulting NCs **5** exhibited similar dimensions indicates well-controlled template synthesis.

Assessment of non-specific interactions of NCs 5 with biomolecules.

The surface layer of NCs **5** contains superhydrophilic zwitterionic SB moieties. Due to the hydration effects of these zwitterionic materials, NCs **5** was expected to have low non-specific interactions with biomolecules.[17, 31] In this study, fibrinogen (from human plasma) was chosen as the model biomolecule, which is a glycoprotein essential for the formation of fibrin-based blood clots.[20, 32] NTA showed that fibrinogen (1 mg/mL in H_2O) itself had a mean D_h of 105 nm (with the peak of the profile at 81 nm). A mixture of fibrinogen (1 mg/mL in H_2O) and NCs **5** (1 mg/mL in H_2O) showed a bimodal profile, with the two peaks corresponding to fibrinogen and NCs **5**, respectively (Figure 3d). In addition, no large particles could be detected immediately after mixing, indicating no aggregation formed during the mixing process. The mixture was allowed to stand for 3 days at room temperature. After 3 days, NTA measurement showed almost the same size profile. The aforementioned results all indicated that non-specific interaction between fibrinogen and NCs **5** was well suppressed.

Evaluation of the stability of NCs 5 in serum.

Serum is the clear liquid separated from clotted blood, which includes all proteins not used in blood clotting (fibrinogens not included), and special components such as antibodies, hormones, antigens. During the blood circulation of nanocarriers, serum may trigger aggregation, and shorten their circulation time. The stability of NCs **5** in fetal bovine serum (FBS, 50% in PBS buffer) was evaluated by monitoring the size change.[33] As shown in Figure S5a, NTA showed similar size profile of NCs **5** in 50% FBS (average D_h: 136 nm) compared with that in H_2O. After incubation of NCs **5** in 50% FBS at 37 °C for 3 days, the size profile essentially remained unchanged (average D_h: 138 nm), indicating the high stability of the NCs **5** in serum. While the crosslinks effectively maintained NCs **5** as integrated nanostructures, the “non-fouling” SB moieties on surface domain of NCs **5** helped to suppress the non-specific interaction between NCs **5** and various components from serum and prevent aggregations.

Biodegradation of NCs 5.

In the presence of proteinase K enzyme (0.2 mg/mL 0.1 M Tris-HCl buffer, pH = 8.5), the NCs **5** (1 mg/mL) was incubated at 37 °C. After 3 days, NTA could not detect any size signal of the NCs **5**, confirming the successful biodegradation. However, we note that NanoSight could not be used for quantitative analysis of the biodegradation process. Related to the current study, the biodegradation behaviors of SB-functionalized PLA (i.e., the structural analogue of the hydrophilic block of **4** and the pendant hydrophilic chains on NCs **5**) and thiol-ene-crosslinked PLA-based NCs (with the crosslinked domains similar to that of NCs **5**) was studied and reported in our previous publications.[14, 20]

In vitro cytotoxicity study.

Both PLA and zwitterions were commonly considered as materials with high biocompatibility.[34, 35] The cytotoxicity of NCs **5** in PaCa-2 pancreatic cancer cells was evaluated by the alamarBlue cell viability assay at 72 h against post treatment of PaCa-2 pancreatic cancer cells (Figure 4). The results showed that NCs **5** (up to 500 μg/mL) was non-toxic in PaCa-2 cells, indicating high biocompatibility of these imaging agents.

In vitro cellular uptake study.

Paca-2 cells were treated with Cy5.5-N_3 and NCs **5** at Cy5.5 concentration of 0.2 μg/mL. Untreated cells were the controls. At 24 h of post treatment, the cellular uptake of NCs **5** in PaCa-2 cells was characterized quantitatively with flow cytometry and qualitatively with confocal microscopy. Flow cytometry data showed that NCs **5** was effectively taken up by PaCa-2 cells (Figure 5a). The mean fluorescence intensity of cells treated by NCs **5** was ~243 folds higher than that of untreated cells (Figure 5b). Confocal microscopy images also confirmed that NCs **5** were successfully taken up by PaCa-2 cells and accumulated inside the cells (Figure 5c). Cy5.5-N_3 treated cells showed stronger fluorescence signals than NCs **5**, which agreed well with previously published work.[30] Although Cy5.5-N_3 showed better cellular uptake efficiency *in vitro*, it mainly accumulated in liver and was not able to reach tumor sites *in vivo*, which was described in details below.

In vivo imaging and biodistribution.

PaCa-2 cells were injected subcutaneously at the flanks of 6-week old female athymic nude mice. When the tumors reached ~300 mm^3, the mice were injected with 0.9% saline (control group), Cy5.5-N_3, or NCs **5** intravenously at Cy5.5 dose of 1.5 mg/kg body weight. Whole body fluorescence imaging using the IVIS *in vivo* imaging system was performed before, 5 min, 1 h, 4 h and 24 h post injection to investigate the biodistributions of Cy5.5-N_3 and NCs **5**. For the mice injected with NCs **5** with images shown in Figure 6a, the NCs **5** distributed across the whole mice body (dorsal side) immediately after injection. After 4 h, fluorescence signals could still be detected throughout the mice body, suggesting that the NCs **5** was circulating during the first 4 hours after injection. At 24 h post injection, from the dorsal side of the mice, only the tumors showed strong fluorescence signals, indicating that NCs **5** successfully accumulated at tumor sites. For the mice injected with Cy5.5-N_3, images of both dorsal side (Figure 6a) and ventral side (Figure S6) of the mice were taken using IVIS imaging system.[36] At 5 min post injection, from the dorsal side, no fluorescence signal was detected, and image from the ventral side showed strong fluorescence signals in liver, suggesting the immediate clearance of Cy5.5-N_3 by liver. At 1 and 4 h post injection, more accumulation of Cy5.5-N_3 in liver (seen from ventral side) and kidney (seen from dorsal side) was observed, indicating the continuous clearance of Cy5.5-N_3 by liver and kidney. Within the 24 h imaging period, no fluorescence signal was ever detected at tumor sites.

Mice were euthanized at 24 h post injection. Tumors and major organs were harvested and imaged by IVIS imaging system (Figure 6b). Besides liver, spleen and kidney, significant fluorescence signals were observed in the tumor of NCs **5** treated mice, indicating that NCs **5** were effective imaging agents for PaCa-2 tumors. In contrast, there was no accumulation

of free Cy5.5-N_3 in the tumors, while fluorescence signals were observed in the liver and kidney.

The above *in vivo* imaging and biodistribution results indicated that the SB/Cy5.5-functionalized NCs **5** exhibited longer circulation time *in vivo* and led to more effective tumor accumulation than the small molecule dye, Cy5.5-N_3. Both nanoscopic dimensions of NCs **5** and the zwitterionic properties of **5**, which promotes colloidal stability of **5** under biological environments, are contribution factors to such results.[37, 38] With their hydrodynamic sizes of ~100 nm, the accumulation of NCs **5** was ascribed to EPR effect. The intensive fluorescence signals from liver and noticeable fluorescence signals from spleen suggested that the reticuloendothelial system (RES) might play a major role in the clearance of NCs **5**, because RES clearance.[39] The fluorescence signals from kidney suggested renal clearance of the population of NCs **5** with relatively small sizes or degraded residues of **5**, because renal clearance mainly functions for objects with size smaller than ~10 nm.[40] For the mice treated with free Cy5.5-N_3, the significant accumulation of Cy5.5-N_3 in kidney and liver sites indicates that both renal clearance and liver uptake are significant pathways to eliminate the dye molecules. Because renal clearance *via* kidney prefers objects with small sizes, the dye molecules cleared through liver uptakes was likely due to larger sized particles. The lower fluorescence intensity in the liver of Cy5.5- N_3 treated mice relative to NCs **5** treated mice might be due to the degradation of small molecule dye in the liver.

CONCLUSIONS

SB/Cy5.5-functionalized crosslinked PLA-based NCs were synthesized and characterized. These NCs showed a series of comprehensive biomedical relevant properties, including colloidal stability, biodegradability, biocompatibility, prolonged *in vivo* circulation time, and effective tumor accumulation (as compared to small molecules). The results suggest that NCs are candidates as cancer imaging agents. Other properties of these NCs may also be useful for other potential biomedical applications in the future, such as individual or co-delivery of drug and gene. While the SB zwitterion was utilized in this work, it should be noted that other zwitterions such as carboxybetaine (CB) and phosphorylcholine (PC) are also valid options of zwitterions,[41] showing that a broad degree of zwitterionic nanostructures can be generated to explore biomedical applications.

Supplementary Material

Refer to Web version on PubMed Central for supplementary material.

ACKNOWLEDGMENT

This work was supported by U. S. National Science Foundation [DMR-1609914; CHE-1412785; CBET-1337860] and U. S. National Institutes of Health [R21 EB024095-01]. The authors thank Prof. Mark T. Swihart and Mr. Zheng Fu for kind support on NTA measurements, Dr. Yueling Qin for technical support on TEM measurements, and UB North Campus Confocal Imaging Facility in the Department of Biological Sciences along with their NSF grant “National Science Foundation MAJOR RESEARCH INSTRUMENTATION Grant # DBI 0923133.

ABBREVIATIONS

NCs	nanocapsules
NPs	nanoparticles
ROP	ring-opening polymerization
NMR	nuclear magnetic resonance
GPC	gel permeation chromatography
NTA	nanoparticle tracking analysis
TEM	transmission electron microscopy

REFERENCES

1. Meier W, Polymer nanocapsules. Chemical Society Reviews 2000, 29, (5), 295–303.
2. Mora-Huertas CE; Fessi H; Elaissari A, Polymer-based nanocapsules for drug delivery. International Journal of Pharmaceutics 2010, 385, (1–2), 113–142. [PubMed: 19825408]
3. Esser-Kahn AP; Odom SA; Sottos NR; White SR; Moore JS, Triggered Release from Polymer Capsules. Macromolecules 2011, 44, (14), 5539–5553.
4. Sun H; Chen C-K; Cui H; Cheng C, Crosslinked polymer nanocapsules. Polym Int 2016, 65, (4), 351–361.
5. Chen C-K; Wang Q; Jones CH; Yu Y; Zhang H; Law W-C; Lai CK; Zeng Q; Prasad PN; Pfeifer BA; Cheng C, Synthesis of pH-Responsive Chitosan Nanocapsules for the Controlled Delivery of Doxorubicin. Langmuir 2014, 30, (14), 4111–4119. [PubMed: 24665861]
6. Tian K; Zeng J; Zhao X; Liu L; Jia X; Liu P, Synthesis of multi-functional nanocapsules via interfacial AGET ATRP in miniemulsion for tumor micro-environment responsive drug delivery. Colloids and Surfaces B: Biointerfaces 2015, 134, 188–195. [PubMed: 26196091]
7. Yan M; Wen J; Liang M; Lu Y; Kamata M; Chen ISY, Modulation of Gene Expression by Polymer Nanocapsule Delivery of DNA Cassettes Encoding Small RNAs. PLoS ONE 2015, 10, (6), e0127986. [PubMed: 26035832]
8. Cheng R; Meng F; Ma S; Xu H; Liu H; Jing X; Zhong Z, Reduction and temperature dual-responsive crosslinked polymersomes for targeted intracellular protein delivery. J. Mater. Chem 2011, 21, 19013–19020.
9. An P; Ba X; Lu S, Preparation and characterization of crosslinked poly(methylmethacrylate) heat sensitive color-developing nanocapsules. Polym. Bull. (Heidelberg, Ger.) 2010, 64, (4), 375–386.
10. Jagielski N; Sharma S; Hombach V; Mailänder V; Rasche V; Landfester K, Nanocapsules Synthesized by Miniemulsion Technique for Application as New Contrast Agent Materials. Macromolecular Chemistry and Physics 2007, 208, (19-20), 2229–2241.
11. Baier G; Musyanovych A; Dass M; Theisinger S; Landfester K, Cross-linked starch capsules containing dsDNA prepared in inverse miniemulsion as "nanoreactors" for polymerase chain reaction. Biomacromolecules 2010, 11, (4), 960–968. [PubMed: 20329746]
12. Landfester K, Miniemulsion Polymerization and the Structure of Polymer and Hybrid Nanoparticles. Angew. Chem., Int. Ed 2009, 48, (25), 4488–4507.
13. Chen C-K; Law W-C; Aalinkeel R; Yu Y; Nair B; Wu J; Mahajan S; Reynolds JL; Li Y; Lai CK; Tzanakakis ES; Schwartz SA; Prasad PN; Cheng C, Biodegradable cationic polymeric nanocapsules for overcoming multidrug resistance and enabling drug-gene co-delivery to cancer cells. Nanoscale 2014, 6, (3), 1567–1572. [PubMed: 24326457]
14. Zou J; Hew CC; Themistou E; Li YK; Chen CK; Alexandridis P; Cheng C, Clicking Well-Defined Biodegradable Nanoparticles and Nanocapsules by UV-Induced Thiol-Ene Cross-Linking in Transparent Miniemulsions. Adv Mater 2011, 23, (37), 4274–4277. [PubMed: 22039596]

15. Sun H; Yarovoy I; Capeling M; Cheng C, Polymers in the Co-delivery of siRNA and Anticancer Drugs for the Treatment of Drug-resistant Cancers. Topics in Current Chemistry 2017, 375, (2), 24. [PubMed: 28176270]

16. Lin G; Hu R; Law W-C; Chen C-K; Wang Y; Chin HL; Nguyen QT; Lai CK; Yoon HS; Wang X; Xu G; Ye L; Cheng C; Yong K-T, Biodegradable Nanocapsules as siRNA Carriers for Mutant K-Ras Gene Silencing of Human Pancreatic Carcinoma Cells. Small 2013, 9, (16), 2757–2763. [PubMed: 23427041]

17. Jiang SY; Cao ZQ, Ultralow-Fouling, Functionalizable, and Hydrolyzable Zwitterionic Materials and Their Derivatives for Biological Applications. Adv Mater 2010, 22, (9), 920–932. [PubMed: 20217815]

18. Jin Q; Chen Y; Wang Y; Ji J, Zwitterionic drug nanocarriers: A biomimetic strategy for drug delivery. Colloids and Surfaces B: Biointerfaces 2014, 124, 80–86. [PubMed: 25092584]

19. Zheng LC; Sun ZJ; Li CC; Wei ZY; Jain P; Wu K, Progress in biodegradable zwitterionic materials. Polym Degrad Stabil 2017, 139, 1–19.

20. Sun H; Chang MYZ; Cheng W-I; Wang Q; Commisso A; Capeling M; Wu Y; Cheng C, Biodegradable zwitterionic sulfobetaine polymer and its conjugate with paclitaxel for sustained drug delivery. Acta Biomater 2017, 64, 290–300. [PubMed: 29030301]

21. Santra S; Dutta D; Walter GA; Moudgil BM, Fluorescent nanoparticle probes for cancer imaging. Technol Cancer Res T 2005, 4, (6), 593–602.

22. Barreto JA; O'Malley W; Kubeil M; Graham B; Stephan H; Spiccia L, Nanomaterials: Applications in Cancer Imaging and Therapy. Adv Mater 2011, 23, (12), H18–H40. [PubMed: 21433100]

23. Meldal M; Tornoe CW, Cu-catalyzed azide-alkyne cycloaddition. Chemical Reviews 2008, 108, (8), 2952–3015. [PubMed: 18698735]

24. Yu Y; Zou J; Yu L; Jo W; Li YK; Law WC; Cheng C, Functional Polylactide-g-Paclitaxel-Poly(ethylene glycol) by Azide-Alkyne Click Chemistry. Macromolecules 2011, 44, (12), 4793–4800.

25. Engler AC; Bonner DK; Buss HG; Cheung EY; Hammond PT, The synthetic tuning of clickable pH responsive cationic polypeptides and block copolypeptides. Soft Matter 2011, 7, (12), 5627–5637.

26. Zeng DY; Kuang GT; Wang SK; Peng W; Lin SL; Zhang Q; Su XX; Hu MH; Wang HG; Tan JH; Huang ZS; Gu LQ; Ou TM, Discovery of Novel 11-Triazole Substituted Benzofuro[3,2-b]quinolone Derivatives as c-myc G-Quadruplex Specific Stabilizers via Click Chemistry. J Med Chem 2017, 60, (13), 5407–5423. [PubMed: 28514170]

27. Tian T; Zhang H-X; He C-P; Fan S; Zhu Y-L; Qi C; Huang N-P; Xiao Z-D; Lu Z-H; Tannous BA; Gao J, Surface functionalized exosomes as targeted drug delivery vehicles for cerebral ischemia therapy. Biomaterials 2018, 150, 137–149. [PubMed: 29040874]

28. Carter KA; Wang S; Geng JM; Luo DD; Shao S; Lovell JF, Metal Chelation Modulates Phototherapeutic Properties of Mitoxantrone-Loaded Porphyrin-Phospholipid Liposomes. Mol Pharmaceut 2016, 13, (2), 420–427.

29. Cai MT; Leng MT; Lu AJ; He L; Xie XX; Huang L; Ma YH; Cao J; Chen YW; Luo XL, Synthesis of amphiphilic copolymers containing zwitterionic sulfobetaine as pH and redox responsive drug carriers. Colloid Surface B 2015, 126, 1–9.

30. Garg SM; Paiva IM; Vakili MR; Soudy R; Agopsowicz K; Soleimani AH; Hitt M; Kaur K; Lavasanifar A, Traceable PEO-poly(ester) micelles for breast cancer targeting: The effect of core structure and targeting peptide on micellar tumor accumulation. Biomaterials 2017, 144, 17–29. [PubMed: 28818703]

31. Chen SF; Li LY; Zhao C; Zheng J, Surface hydration: Principles and applications toward low-fouling/nonfouling biomaterials. Polymer 2010, 51, (23), 5283–5293.

32. Wang LG; Yang QH; Cui YS; Gao DW; Kang JX; Sun HT; Zhu LL; Chen SF, Highly stable and biocompatible dendrimerencapsulated gold nanoparticle catalysts for the reduction of 4-nitrophenol. New J Chem 2017, 41, (16), 8399–8406.

33. Lin W; Ma G; Kampf N; Yuan Z; Chen S, Development of Long-Circulating Zwitterionic Cross-Linked Micelles for Active-Targeted Drug Delivery. Biomacromolecules 2016, 17, (6), 2010–2018. [PubMed: 27050797]

34. Yu Y; Zou J; Cheng C, Synthesis and biomedical applications of functional poly(alpha-hydroxyl acid)s. Polym Chem 2014, 5, (20), 5854–5872.

35. Zheng LC; Sundaram HS; Wei ZY; Li CC; Yuan ZF, Applications of zwitterionic polymers. React Funct Polym 2017, 118, 51–61.

36. Cordero AB; Kwon Y; Hua X; Godwin AK, In vivo Imaging and Therapeutic Treatments in an Orthotopic Mouse Model of Ovarian Cancer. Journal of Visualized Experiments : JoVE 2010, (42), 2125. [PubMed: 20811322]

37. Wang B; He X; Zhang ZY; Zhao YL; Feng WY, Metabolism of Nanomaterials in Vivo: Blood Circulation and Organ Clearance. Accounts Chem Res 2013, 46, (3), 761–769.

38. Chen Y; Li Z; Wang H; Wang Y; Han H; Jin Q; Ji J, IR-780 Loaded Phospholipid Mimicking Homopolymeric Micelles for Near-IR Imaging and Photothermal Therapy of Pancreatic Cancer. ACS Applied Materials & Interfaces 2016, 8, (11), 6852–6858. [PubMed: 26918365]

39. Petros RA; DeSimone JM, Strategies in the design of nanoparticles for therapeutic applications. Nat Rev Drug Discov 2010, 9, (8), 615–627. [PubMed: 20616808]

40. Longmire M; Choyke PL; Kobayashi H, Clearance properties of nano-sized particles and molecules as imaging agents: considerations and caveats. Nanomedicine-Uk 2008, 3, (5), 703–717.

41. Shao Q; Jiang SY, Molecular Understanding and Design of Zwitterionic Materials. Adv Mater 2015, 27, (1), 15–26. [PubMed: 25367090]

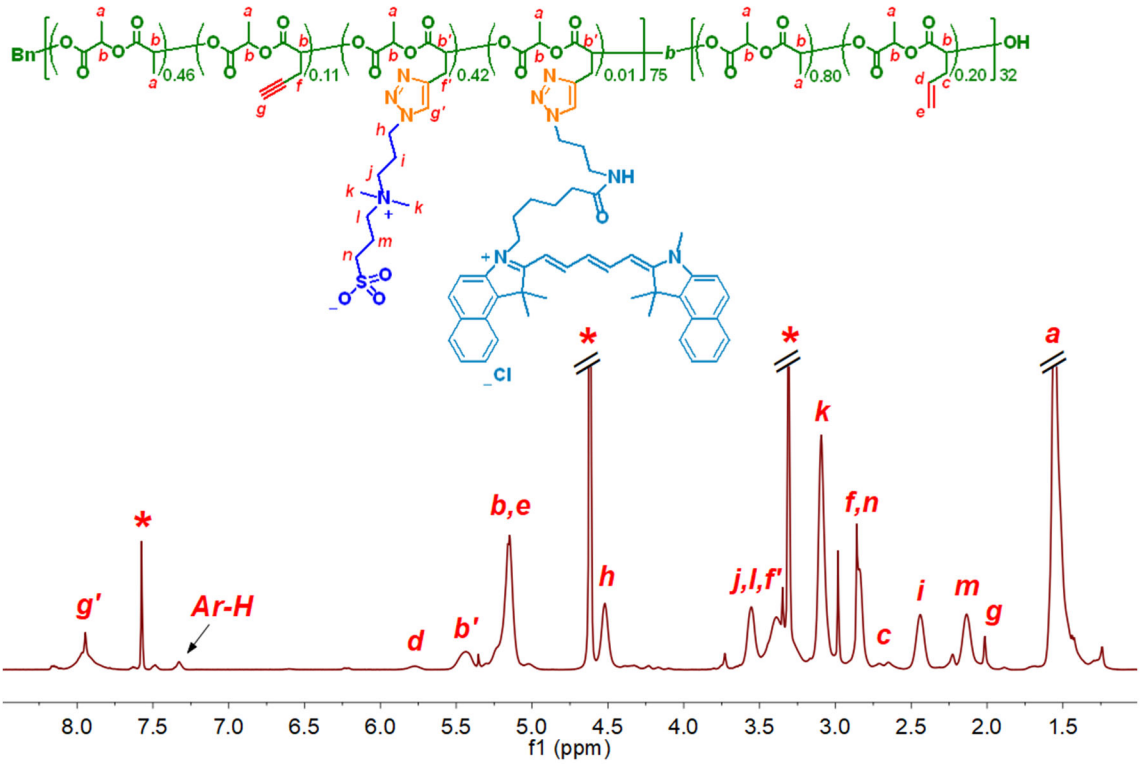

Figure 1.

Structure and ^{1}H NMR spectrum of **4** in $CDCl_3/CD_3OD$ (v/v, 1:1).

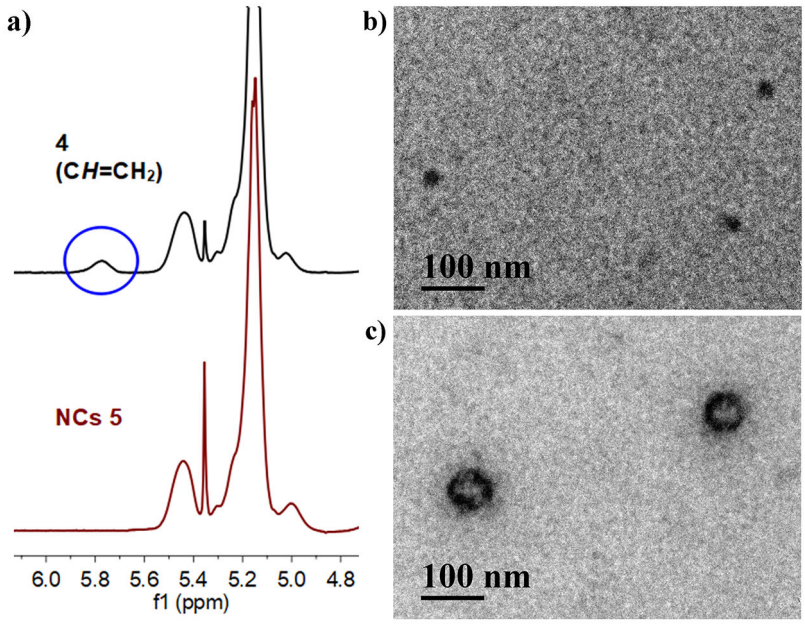

Figure 2.

a) Partial ^{1}H NMR spectra of **4** and NCs **5** in $CDCl_3/CD_3OD$ (v/v, 1:1). b) TEM image of NPs of **4**. c) TEM image of NCs **5**. TEM samples were stained with RuO_4 before measurements.

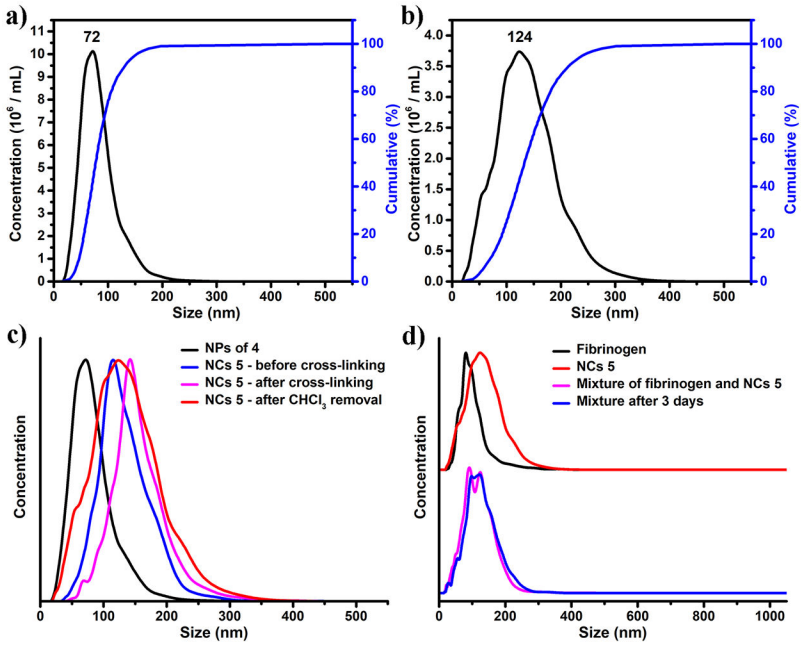

Figure 3.

Size distribution profiles based on NTA measurements: a) NPs of **4** in H_2O. b) NCs **5** in H_2O. c) NCs **5** on different steps of synthesis. d) Fibrinogen, NCs **5**, and the mixture of these two before and after 3 days incubation.

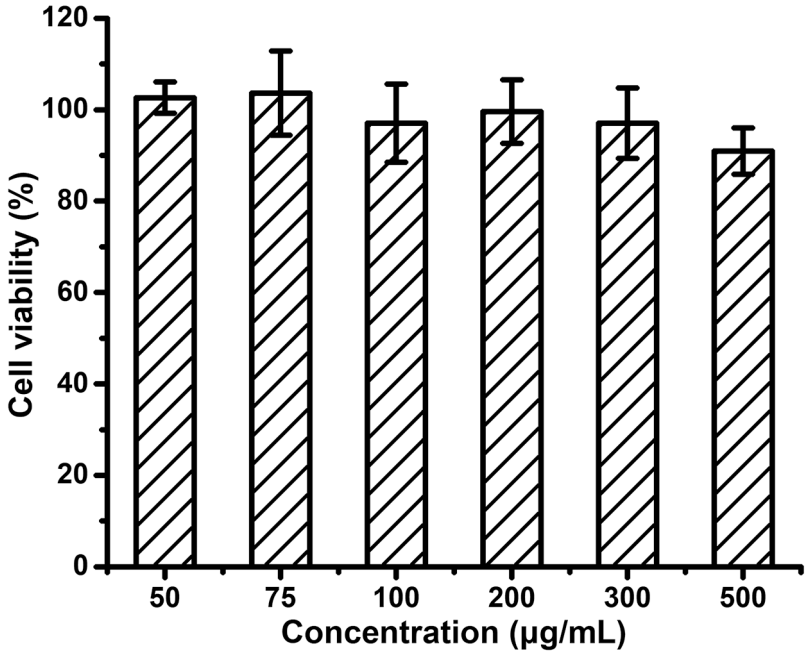

Figure 4.

Cytotoxicity of NCs **5** in PaCa-2 cells. Paca-2 cells were treated with NCs **5** at concentrations of 50, 75, 100, 200, 300 and 500 ug/mL. The cell viability was measured at 72 h post treatment. (n = 3)

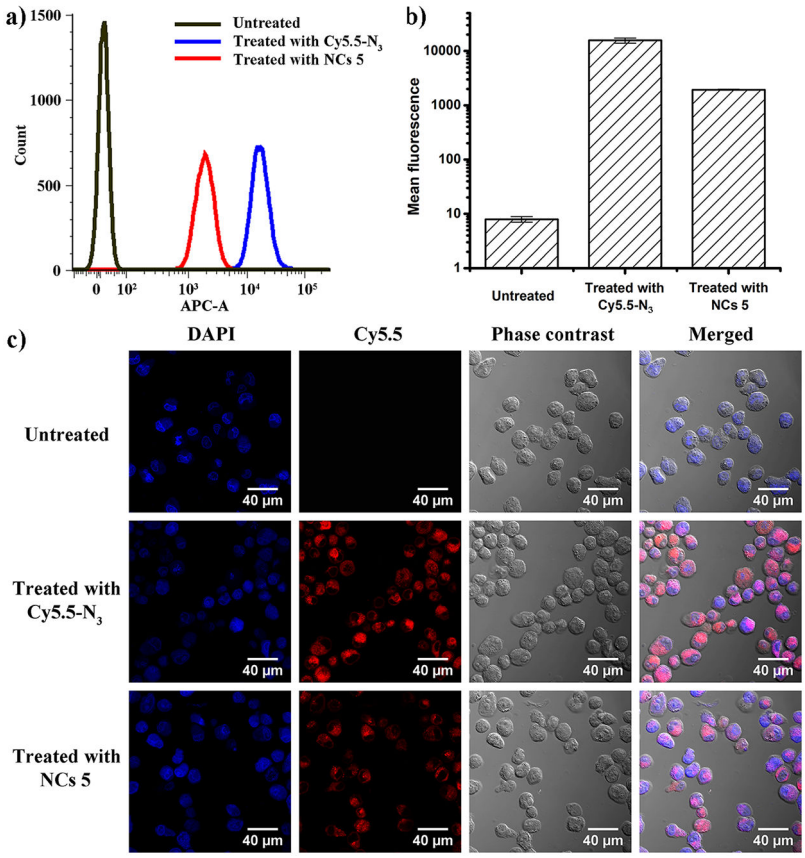

Figure 5.

a) A typical set of flow cytometry data showing uptake of Cy5.5-N_3 and NCs **5** in PaCa-2 cells at 24 h post treatment. b) Mean fluorescence intensity of Cy5.5 obtained from flow cytometry (n = 3). c) Confocal microscopy images of PaCa-2 cells at 24 h post treatment with Cy5.5-N_3 and NCs **5**. Cell nuclei were counterstained with DAPI.

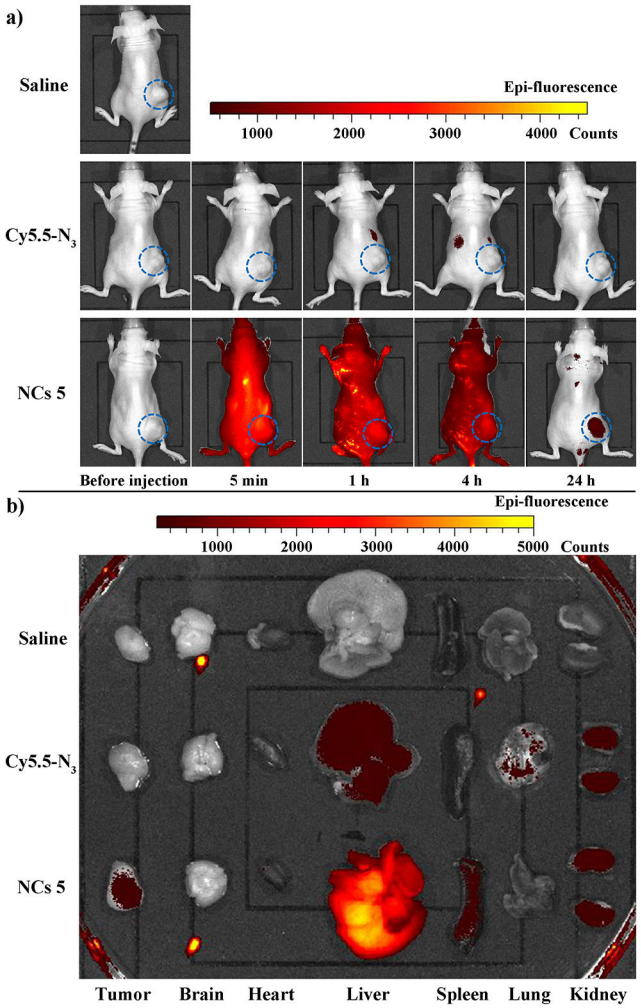

Figure 6.

a) Whole body fluorescence imaging of mice (dorsal side) before and at different time points post intravenous injection of saline, Cy5.5-N_3, NCs **5** at Cy5.5 dose of 1.5 mg/kg body weight. Tumors are circled in each figure. b) *Ex vivo* fluorescence imaging of tumors and major organs at 24 h post intravenous injection of saline, Cy5.5-N_3, NCs **5**.

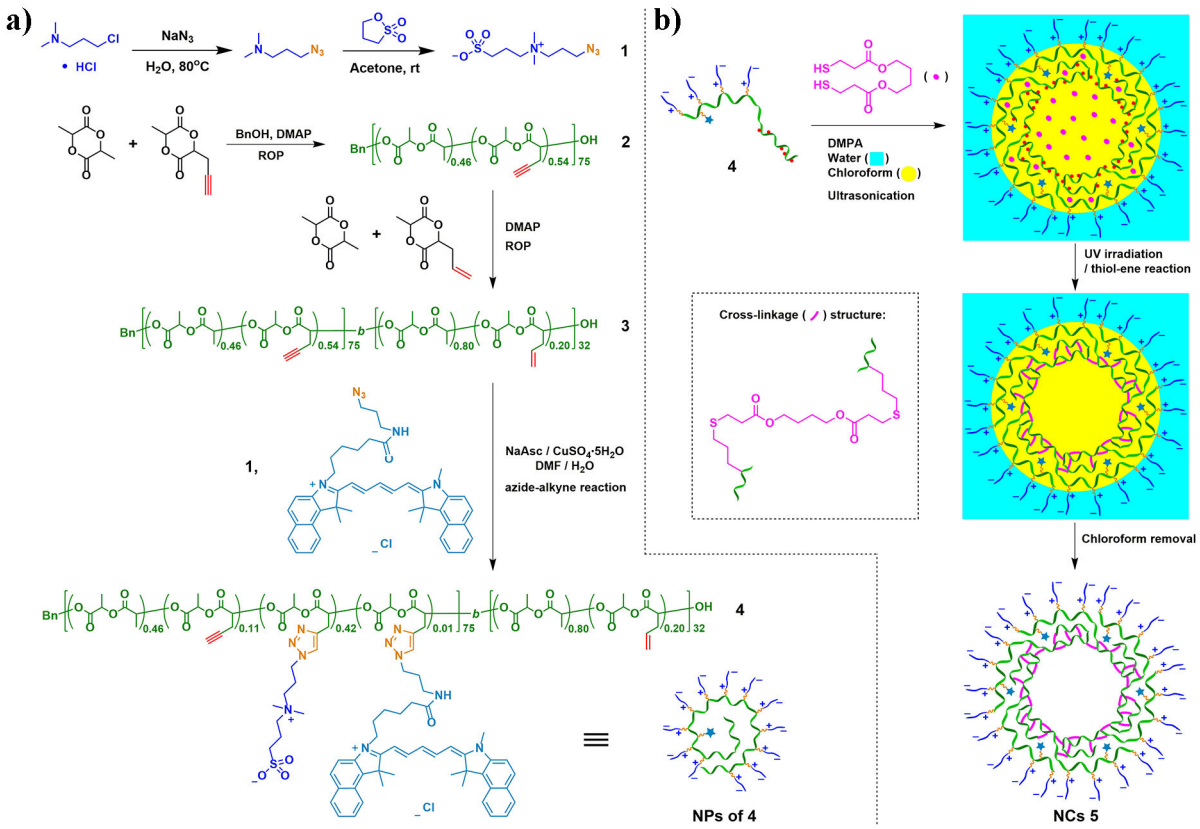

Scheme 1.

a) Synthesis of the PLA-based diblock copolymer **4** with a hydrophilic SB/Cy5.5-functionalized block and a hydrophobic allyl-functionalized block. b) Transformation of **4** into crosslinked NCs **5**.